> ASC2024-4LPo1C-02 <

Topology Optimization of a Fully Superconducting Air-core Motor for Electric Aircraft

Wenkai Yan, Xiaoze Pei, *Senior Member, IEEE*, Han Wang, Yuchen Wang, John Frederick Eastham, Xianwu Zeng, *Member, IEEE*

***Abstract*—Superconducting motors have great potential to achieve high power density and high efficiency in electric propulsion systems for aerospace applications. A new lightweight air-core topology for a fully superconducting motor is designed and optimized. The stator is made of yttrium barium copper oxide (YBCO) cable and has two sets of windings. These are spatially displaced radially and have a specific circumferential offset to cancel certain harmonics. The rotor is also constructed with YBCO cable. This paper focuses on the optimization of superconducting motor windings in terms of winding harmonics. The topology of the stator and rotor is designed through a series of analytical calculations and comparisons. Four superconducting motor topologies with different pole numbers are presented with detailed design for the stator and rotor windings. An illustration of how the harmonics reduction design methodology is applied is included. The analytical design is verified by a 2D finite element model of the superconducting motor using the COMSOL software. The topology optimization using analytical calculations can effectively reduce the superconductor motor design iterative process and time.**

***Index Terms*—Superconducting motor, airgap winding design, electric aircraft (EA), electric propulsion system (EPS).**

I. INTRODUCTION

As the demand for air traffic continues to grow in the coming decades, the Strategic Research and Innovation Agenda (SRIA) has set specific emission and noise reduction targets to address this problem [1]. Electrified aircraft are of critical importance to achieve these goals [2]. Advanced Superconducting and Cryogenic Experimental powertraiN Demonstrator (ASCEND) demonstrated great potential for applying cryogenic and superconducting technologies for hydrogen-powered aircraft [3][4]. Superconducting motors are more efficient, smaller, and lighter than conventional motors. The application of high-temperature superconducting motors for electric aircraft is now feasible [5][6]. A superconducting motor with double layer winding can have stable torque production and negligible space harmonics [7][8]. Air-core superconducting motors are more beneficial for aerospace applications than those with iron cores [9][10][11]. Due to the coreless design, the high magnetic field will not cause saturation, and there are no iron losses [12], the weight is reduced while increasing the power density of the motors, which allows them to be lighter and more efficient [13] [14]. A fully superconducting air-core machine for aircraft propulsion has been proposed [15].

This paper explores the analytical design of the stator and rotor for a superconducting air-core motor. A double layer winding is used in this design and the benefit is analyzed. Analytical methods are used to optimize winding design, reducing simulation and design time. The analytical calculation method derivation is also elaborated. The derivation of these methods is detailed, and a new fully superconducting air-core motor topology is designed and validated using 2D finite element simulation.

Manuscript received Month xx, 2xxx; revised Month xx, xxxx; accepted Month x, xxxx. This work was supported in part by the UK EPSRC Open Fellowship EP/W033941/1 - Towards Zero Emissions Electric Aircraft through Superconducting DC Distribution Network.

Wenkai Yan, Xiaoze Pei, Yuchen Wang and John Frederick Eastham are with the Dept. of Electronics & Electrical Engineering, University of Bath, Bath, BA2 7AY, United Kingdom. (e-mail: X.Pei@bath.ac.uk).

Han Wang and Xianwu Zeng are with the Dept. of Mechanical Engineering, University of Bath, Bath, BA2 7AY, United Kingdom.

II. MOTOR WINDING TOPOLOGY

Conventional motor windings are typically centralized or modular and placed in slots made of ferromagnetic materials, with all the coils in the same plane. The magnetic field generated by the winding affects the saturation level of ferromagnetic materials. Airgap windings are different from conventional motor windings, without ferromagnetic material support structure, allowing the windings to be distributed in different planes, ignoring the limitations imposed by the saturation of ferromagnetic materials [16]. Because a high magnetic field will be created by superconducting winding, airgap windings are used in this study to achieve high power density.

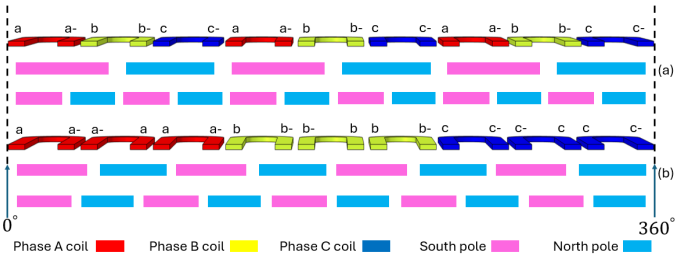

Fig. 1. Single layer stator windings in linear form

Two forms of the single layer stator winding are presented in the linear form as shown in Fig. 1. In Fig. 1(a), the 9-coil airgap winding can generate 6-pole and 12-pole fields using three of

3-coil groups while the 3-coil airgap winding can generate 2/4-pole principal magnetic fields. Alternatively, the 9-coil winding shown at Fig. 1(b) produces 8/10-pole fields.

This paper will specifically investigate the 9-coil 6/12-pole and 9-coil 8/10-pole windings. As the 9-coil 6/12-pole is obtained by repeating the 3-coil 2/4-pole three times, in the subsequent section, the calculation will use the 3-coil 2/4-pole to represent the study of 9-coil 6/12-pole.

A. Stator design

1) **Winding factor for airgap winding in stator**

In slotted machines, the winding harmonic conductor distribution is generally considered using point conductors modelling the slot conductors. This is inappropriate for airgap windings which have broad coil sides in the airgap and must be modelled by thin broad conductor distributions of the same width as the coil sides. If a coil side at θ_s is 2δ wide and has N_s conductors, the p_{th} harmonic of the winding distribution is given by:

$$\bar{N}_P = \frac{1}{\pi}\int_{\theta_{s-\delta}}^{\theta_{s+\delta}} \frac{N_s}{2\delta}\varepsilon^{-jp\theta_s} = \frac{1}{\pi}\frac{\sin p\delta}{p\delta}N_s\varepsilon^{-jp\theta_s} \quad (1)$$

The stator winding has 3 phases, so the magnetic field produced by each phase must be summed, making the calculation more complex. A simplified calculation of the distribution factor on the stator side is given by Eastham [16] [17]. The calculation process is discussed here. It needs to be carried out in steps to determine the winding factor of a completed airgap winding. Firstly, the distribution factor of each individual coil is calculated. Then, the effect of all coils in the same phase is considered. The distribution factor of a single coil is obtained by multiplying the chording factor, which accounts for the coil pitch being shorter than the pole pitch. The coil centers are not displaced by whole harmonic pole pitches, requiring a group factor to account for these effects. Thus, the winding factor for airgap winding can be calculated by:

$$w_{pf} = w_{pfb}\, w_{pfp} w_{pfg} \quad (2)$$

where w_{pfb} is breadth factor, w_{pfp} is pitch factor, and w_{pfg} is group factor.

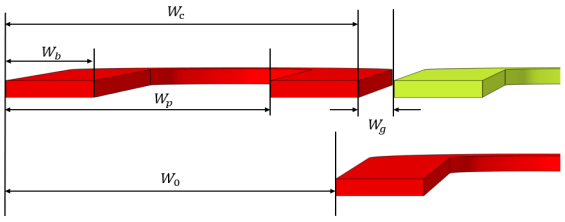

Fig. 2. Parameter definition of airgap winding in linear form

Fig. 2 shows the concept of airgap windings in linear form. When all the coils are exactly next to each other so that the distance between them: $w_g = 0$, $w_c = L/N$ where N is the number of coils in the winding and L is the circumference of the motor.

The coefficient $k = \frac{w_b}{w_c}$ represents the ratio of winding width to the coil width. Therefore, the expression for coil pitch can be obtained as, $w_p = w_c - w_b = w_c(1-k)$. The expressions for w_{pfb} and w_{pfp} can then be calculated [17].

$$w_{pfb} = \frac{L}{pw_b\pi}\sin\frac{pw_b\pi}{L} \quad (3)$$

$$w_{pfp} = \sin\frac{p\pi w_p}{L} \quad (4)$$

Substituting $w_c = L/N$, $w_b = w_c k$ and $w_p = w_c - w_b = w_c(1-k)$ into equations (4) and (5):

$$w_{pfb} = \frac{LN}{pk\pi}\sin\frac{pk\pi}{N} \quad (5)$$

$$w_{pfp} = \sin\frac{p\pi(1-k)}{N} \quad (6)$$

The group winding factor must be considered for each phase that has more than one coil. It can be calculated considering the position of each coil in electrical degrees. Assume there are n-coil for each phase, and their electrical angles are: 0, α_2, $\alpha_3 \ldots \alpha_n$. If the current in the coil flows in the same direction as in the first coil, a positive sign is used. If the current flows in the opposite direction, a negative sign is used. Thus, the w_{pfg} can be expressed as:

$$w_{pfg} = \frac{e^{-j0} \pm e^{-ja_2} \pm e^{-ja_3} \ldots\ldots e^{-ja_n}}{n} \quad (7)$$

As shown in Fig. 1, there are 3 coils in each phase for the 9-coil 8/10-pole. The first coil is at an electrical angle of zero and serves as a reference for the direction of the current. The electrical angle of the second coil is $2\pi p/9$, where p is the harmonic pole number. According to the analysis above, since in the second coil, the current flows in the opposite direction to the first, the corresponding $e^{-j\alpha}$ has a negative sign. Similarly, the third one is positive. Therefore, the w_{pfg9} can be expressed as below for the total harmonics generated by the nine coils□

$$w_{pfg9} = \frac{e^{-j0} - e^{-j\frac{2\pi p}{9}} + e^{-j\frac{4\pi p}{9}}}{n} = \frac{2\cos(2\pi p/9) - 1}{3} \quad (8)$$

For 3-coil 2-pole and 4-pole, each phase has one coil, so the $w_{pfg3} = 1$.

Table I to IV show the analytical results of the winding factor for the airgap windings 3-coil 2-pole and 4-pole, 9-coil 8-pole and 10-pole.

TABLE I
WINDING FACTOR OF 3-COIL 2-POLE HARMONIC

k	ω_{pfb}	ω_{pfp}	ω_{pfg}	ω_{pf}
0.05	0.999	0.839	1	0.838
0.15	0.996	0.777	1	0.774
0.25	0.989	0.707	1	0.699
0.35	0.978	0.629	1	0.615
0.45	0.963	0.545	1	0.525

TABLE II
WINDING FACTOR OF 3-COIL 4-POLE HARMONIC

k	ω_{pfb}	ω_{pfp}	ω_{pfg}	ω_{pf}
0.05	0.998	0.914	1	0.912
0.15	0.984	0.978	1	0.962
0.25	0.955	1	1	0.955
0.35	0.913	0.978	1	0.893
0.45	0.858	0.914	1	0.784

TABLE III
WINDING FACTOR OF 9-COIL 8-POLE HARMONIC

k	ω_{pfb}	ω_{pfp}	ω_{pfg}	ω_{pf}
0.05	0.999	0.970	0.960	0.931
0.15	0.993	0.927	0.960	0.883
0.25	0.980	0.866	0.960	0.814
0.35	0.961	0.788	0.960	0.727
0.45	0.935	0.695	0.960	0.624

TABLE IV
WINDING FACTOR OF 9-COIL 10-POLE HARMONIC

k	ω_{pfb}	ω_{pfp}	ω_{pfg}	ω_{pf}
0.05	0.999	0.996	0.960	0.955
0.15	0.989	0.996	0.960	0.945
0.25	0.969	0.967	0.960	0.898
0.35	0.939	0.906	0.960	0.817
0.45	0.900	0.819	0.960	0.708

Tables I to IV show that the smaller the value of k, the larger winding factor w_{pf}. However, the number of conductors that can be accommodated at a certain coil width w_c would decrease, and the resulting magnetic field is subsequently reduced. Therefore, k = 0.25 is selected for the motor designs because of reasonable high winding factor and sufficient width for conductors.

2) **Double layer offset winding**

Single layer winding generates a magnetic field with the fundamental magnetic field producing torque to drive the motor together with other unwanted harmonics. Harmonics cause two unwanted effects: an increase in synchronous reactance and losses in the magnetic shield between stator and rotor due to their different rotation speeds. A second layer of winding is introduced to reduce these effects. This second layer is offset by a specific angle, so that the sum leaves the wanted drive harmonic at the same value but cancels the larger unwanted harmonic distributions [16] [17].

The magnitude of the conductor distribution from the pair of windings can be calculated as the number of equivalent conductors $\bar{N}_{pat}$. Assuming that $\bar{N}_{pa}$ is the conductor distribution from the first layer phase winding then if a second layer of winding that is identical to the first layer is added and has a physical offset of w_0, the overall winding distributions can be found as follows:

When the second set of windings is energized by a current in the same direction as the first:

$$\bar{N}_{pat} = \bar{N}_{pa}\,(1 + \varepsilon^{-j2\pi w_0 p/L}) = \bar{N}_{pa} 2\varepsilon^{-jpw_0\pi/L}\cos(pw_0\pi/L) \quad (9)$$

When the current through the second set of windings is reversed from the first:

$$\bar{N}_{pat} = \bar{N}_{pa}\,(1 - \varepsilon^{-j2\pi w_0 p/L}) = \bar{N}_{pa} 2\varepsilon^{-jpw_0\pi/L}\sin(pw_0\pi/L) \quad (10)$$

From the equations above, it can be concluded that the amplitude of the magnetic field generated by the winding is multiplied by $|2\cos(pw_0\pi/L)|$, when the current is in the same direction and by $|2\sin(pw_0\pi/L)|$, when the current is reversed.

w_0 the mechanical offset of the second winding, is given by the following equation:

$$w_0 = \frac{nL}{2p} \quad (11)$$

where L is the circumference of the winding, p is the number of pole pairs corresponding to the harmonics to be cancelled, and n is an integer.

When the offset is applied and the direction of the current flow is the same, n can be any odd positive integer. On the other hand, when the current flow direction is reversed with respect to the first layer of winding, n can be any even positive integer. For p_{th} harmonic having a wavelength L/p, the offset can strengthen the fundamental harmonic while minimizing the amplitude of the unwanted p_{th} harmonic.

In this paper, π is chosen for the mechanical offset, because in 9-coil 6/12-pole and 9-coil 8/10-pole, the desired cancellation of specific harmonics can be achieved with this offset. Table V and VI show the result of the winding factor of double layer 9-coil 6/12-pole and 9-coil 8/10-pole at k = 0.25.

TABLE V
WINDING FACTORS OF 9-COIL 6/12-POLE

Pole pair number	Single layer	Double layer offset 6 pole	Double layer offset 12 pole
3	0.699	0.699	0
6	0.955	0	0.955
12	0	0	0
15	0.522	0.522	0
21	0.373	0.373	0
24	0	0	0

TABLE VI
WINDING FACTORS OF 9-COIL 8/10-POLE

Pole pair number	Single layer	Double layer offset 8 pole	Double layer offset 10 pole
1	0.0458	0	0.0458
2	0.108	0.108	0
4	0.814	0.814	0
5	0.898	0	0.898
7	0.197	0	0.197
8	0.141	0.141	0

B. Rotor design

The rotor design uses simple airgap wound coils with DC excitation, the DC winding calculation is illustrated below. Eq. (1) is used to calculate the conductor distribution and hence the

magnetic field generated by the rotor winding.

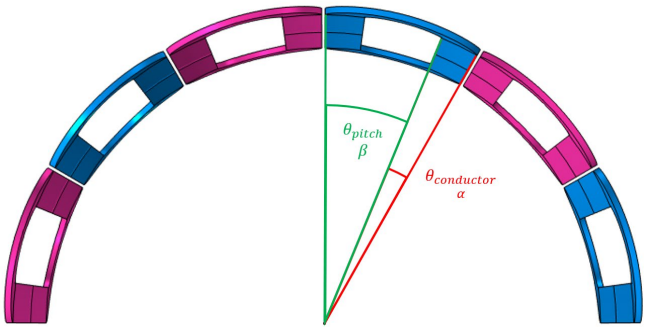

Fig. 3. Definition of angles of conductor, e.g. α = 25%, β = 75%

The overall mechanical angle of the motor is 360 degrees. A 12-pole magnetic field needs to be generated from the rotor, therefore each pole of the magnetic field has a mechanical angle of 36 degrees. Two scaling coefficients α and β are used to represent the ratio of winding width and pitch. As shown in Fig. 3, where α refers to the ratio of conductor width to the mechanical angle of each pole. β refers to the ratio of the mechanical angle between the pitch of each pair of conductors to the mechanical angle of each pole.

$$\theta_{pole} = \frac{360}{2p} \tag{12}$$

$$\alpha = \frac{\theta_{conductor}}{\theta_{pole}} \tag{13}$$

$$\beta = \frac{\theta_{pitch}}{\theta_{pole}} \tag{14}$$

where θ_{pitch} refers to the coil span and $\theta_{conductor}$ refers to the conductor width. Both θ_{pitch} and $\theta_{conductor}$ are limited by performance of the motor and mechanical requirements.

α will change the mechanical angle of the conductor in space, which leads to a change in the position of its electrical angle. This change will have an effect on the conductor distribution, and similarly,when the conductor width is taken into consideration, β will also have an effect. Hence both α and β affect both the conductor distribution and the resultant magnetic field produced by the winding.

Based on the stator design results and considering both the minimum bending radius of the high-temperature superconductor (HTS) winding and the number of pole pairs, the minimum radius of the rotor is 191 mm. Initially, a conductor width of α = 25% is selected for the rotor. In this case, 12 Conductor on Round Core (CORC) HTS cables can be accommodated. Subsequently, the impact of α and β on the magnetic field is investigated, keeping the number of conductors fixed.

Table VII and VIII shows the rotor winding harmonics for β of 66.6% and 75% with α from 10% to 25%. This is because with a fixed number of conductors, a smaller θ_{center} cannot meet the bending angle of the HTS and a larger θ_{center} is not suitable for the existing conductor number.

TABLE VII
ROTOR WINDING HARMONICS FOR β =75%

Harmonic / α	1	3	5	7	9	11
25%	0.5540	0.0765	0.0459	0.0791	0.0616	0.0209
20%	0.5590	0.0772	0.0463	0.0799	0.0621	0.0211
15%	0.5630	0.0778	0.0467	0.0805	0.0626	0.0212
10%	0.5660	0.0782	0.0469	0.0809	0.0629	0.0213

TABLE VIII
ROTOR WINDING HARMONICS FOR β =66.6%

Harmonic / α	1	3	5	7	9	11
25%	0.5190	0	0.1040	0.0742	0	0.0472
20%	0.5240	0	0.1050	0.0749	0	0.0477
15%	0.5280	0	0.1060	0.0754	0	0.048
10%	0.5310	0	0.1060	0.0758	0	0.0482

From TABLE VII and VIII, with α = 25%, the fundamental content of β = 75% is greater than β = 66.6% and also the amplitudes of the 5th and 7th harmonics are lower. While α remains constant and β is reduced to 66.6%, the third harmonic harmonics increases. If α is less than 25%, the amplitude of the fundamental magnetic field increases, but this reduces the number of conductors, which would decrease the amplitude of the fundamental magnetic field. Therefore, α = 25% is chosen as the conductor width of the rotor, since it gives the best results when β = 75%.

III. FINITE ELEMENT SIMULATION

The FE model is built based on the COMAOL software; by using the results from the analytical calculation, four prototypes of fully superconducting air-core motors are simulated in 2D. The stator and rotor winding currents are 707 A-rms and 2855 A-dc, respectively. Fig. 4 and Fig. 5 show the outline of the 9-coil 12-pole prototype and its magnetic field distribution as an example.

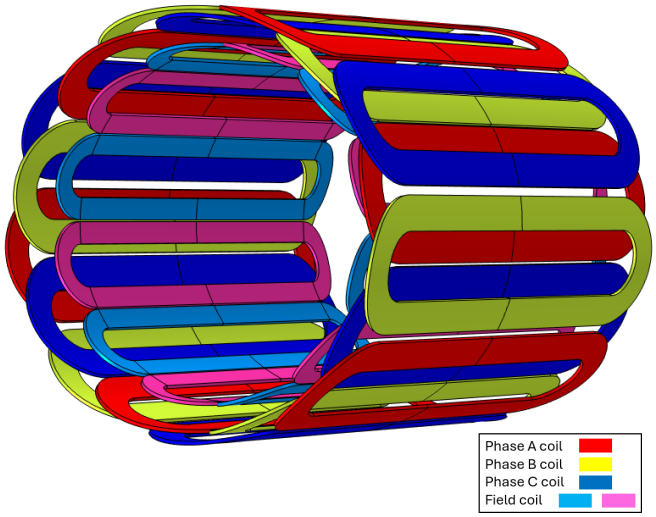

Fig. 4. Motor topology with double layer offset stator winding

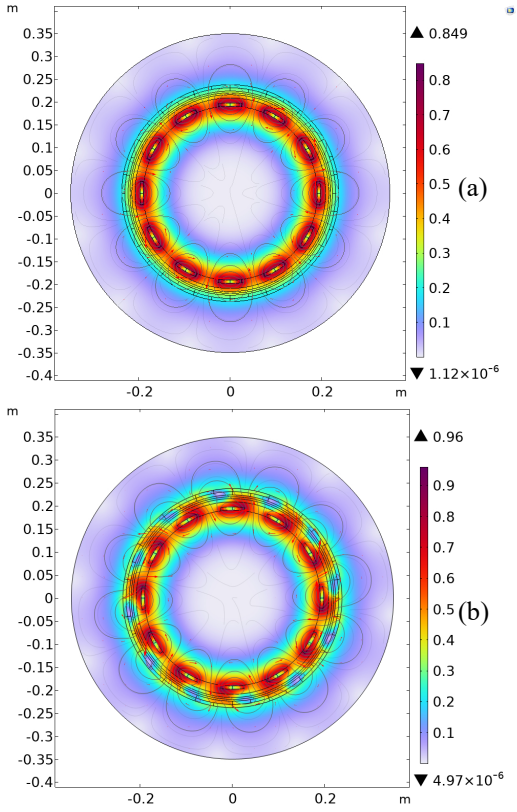

Fig. 5. Magnetic field distribution of 9-coil 12-pole (a) No load condition (b) Full load condition

A. Stator double layer offset winding

Fig. 6 and Fig. 7 show the Fourier analysis of the magnetic fields in the middle of the airgap for windings using the 9-coil 8/10-pole arrangement of Fig.1(b), in both single and double layer form. If the stator has single layer winding it generates both an 8/10-pole field. In this design, only the 10-pole magnetic field needs to be retained to match the rotor winding, so the 8-pole magnetic field needs to be cancelled. After adding the second layer winding offsetting by 180 degrees in mechanical angle and energizing it with reverse current, the 10-pole magnetic field almost doubles and the 8-pole magnetic field is almost eliminated. The simulation result gives the same trend as the analytical calculation.

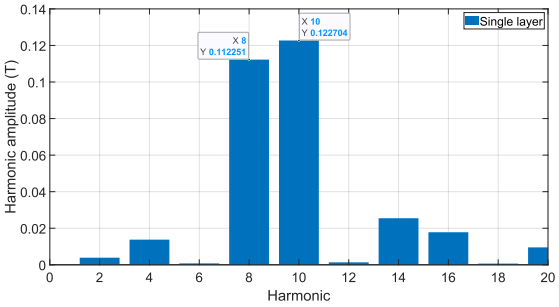

Fig. 6. FFT analysis of 10-pole single layer stator winding

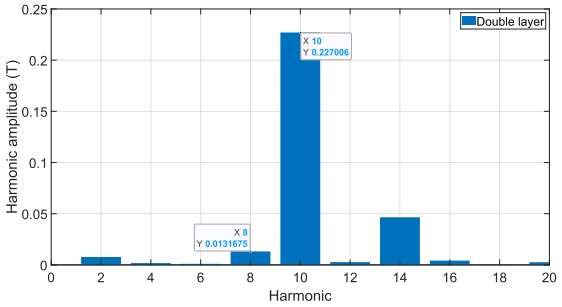

Fig. 7. FFT analysis of 10-pole double layer stator winding

Fig. 8 and Fig. 9 show the Fourier analysis of 9-coil 6/12-pole stator single and double layer winding magnetic fields in the middle of the airgap. The single layer generates 6/12-pole fields as shown at Fig.8. The stator is intended for use with a 12-pole rotor, so it is necessary to add a second layer of offset windings to cancel the 6-pole field. An offset at a mechanical angle of 180 degrees achieves this and almost doubles the magnitude of the 12-pole field as shown at Fig.9.

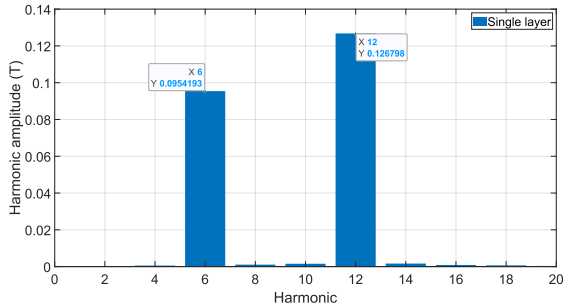

Fig. 8. FFT analysis of 12-pole single layer stator winding

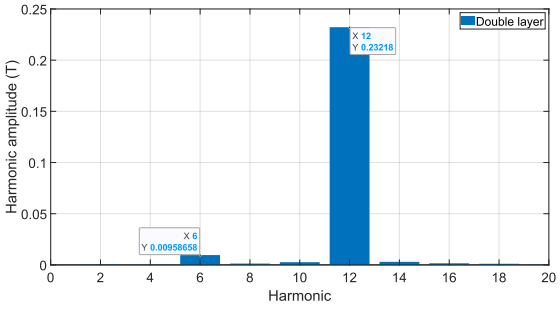

Fig. 9. FFT analysis of 12-pole double layer stator winding

B. Rotor magnetic field analysis FFT

Fig. 10 to Fig. 13 show that at β = 66.6%, the third harmonic in both the 10-pole field and the 12-pole field is significantly reduced. However, it can also be observed that the 5th and 7th harmonic is also increased, which follows the same trend as that calculated in the analytical calculation above. At the same time, with other parameters remaining the same, the fundamental magnetic field generated by the 12-pole is greater than that generated by the 10-pole. Those simulation results correspond with the analytical calculations above. Therefore, 12-pole with

β=75% is selected for the best option.

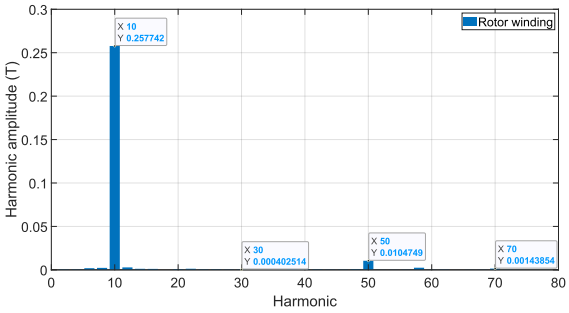

Fig. 10. FFT analysis of 10-pole rotor field with β = 66.6%

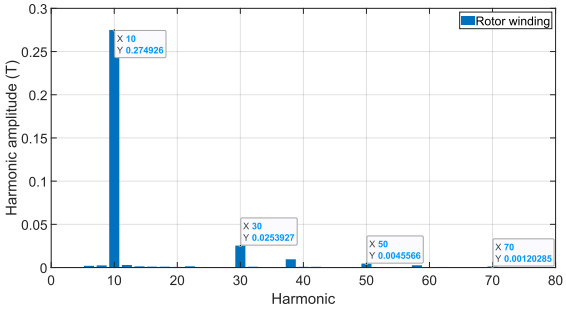

Fig. 11. FFT analysis of 10-pole rotor field with β = 75%

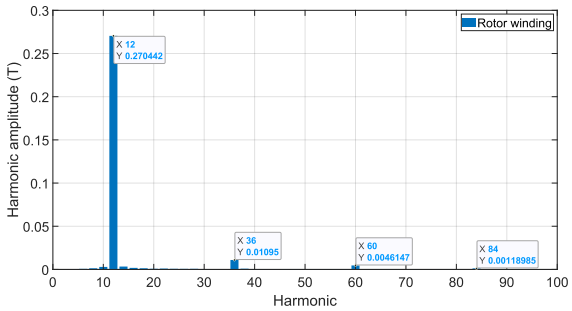

Fig. 12. FFT analysis of 12-pole rotor field with β = 66.6%

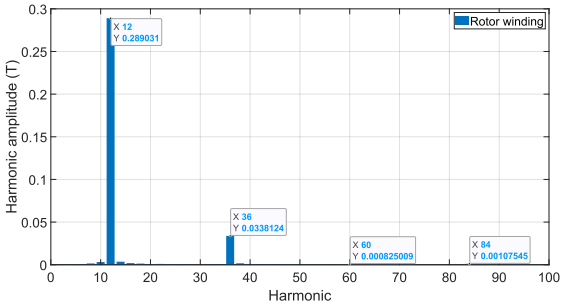

Fig. 13. FFT analysis of 12-pole rotor field with β = 75%

C. Motor performance

Fig. 14 shows that the motor has the highest electromagnetic torque using the 12-pole, β=75% configuration. Overall, the 12-pole, β =75% case is still the best option among the four cases. Fig. 15 shows the waveform of the terminal voltage and input current.

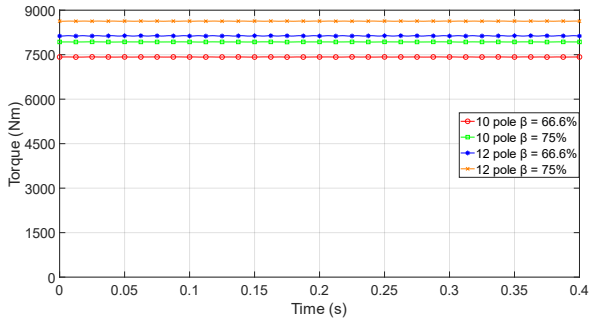

Fig. 14. Electromagnetic torque

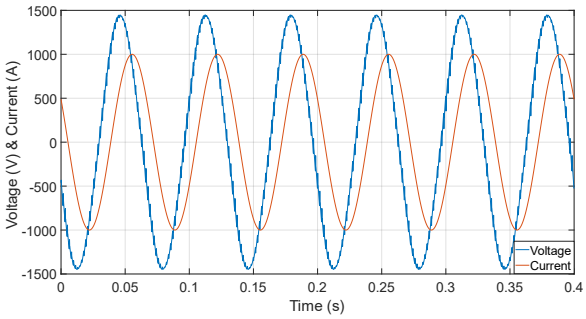

Fig. 15. Voltage and current of 9-coil 12-pole at β = 75%

IV. Conclusion

This paper investigates a fully superconducting motor using air-core topology for electric aircraft propulsion. A double layer winding is proposed for the stator to cancel undesired low-order winding harmonics. The analytical analysis is derived for airgap windings and then used for superconducting motor winding optimization. The stator winding with 9-coil 12-pole has the highest winding factor among all the 9-coil possible pole numbers. The 2D finite element modeling results are consistent with the analytical calculations, which validates the motor design methodology. The analytical calculations can be used directly to predict the optimized motor topology, which significantly reduces the simulation time required for motor design.

REFERENCES

[1] "Advisory Council for Aviation Research and Innovation in Europe," *Advisory Council for Aviation Research and Innovation in Europe*, 2024. Available: https://www.acare4europe.org. [Accessed: Mar. 06, 2024]

[2] J. Gieras, "Superconducting Electrical Machines - State of the Art," *Przegląd Elektrotechniczny*, vol. 85, no. 12, pp. 1–19, Jan. 2009.

[3] L. Ybanez et al., "ASCEND: The first step towards cryogenic electric propulsion," IOP conference series, vol. 1241, no. 1, pp. 012034–012034, May 2022, doi: https://doi.org/10.1088/1757-899x/1241/1/012034

[4] L. Ybanez et al., "Cryogenic electric propulsion system: ASCEND main results and perspectives," in International Conference on More Electric Aircraft (MEA24), Toulouse, FR, 2024.

[5] C. C. T. Chow, M. D. Ainslie, and K. T. Chau, "High temperature superconducting rotating electrical machines: An overview," *Energy Reports*, vol. 9, pp. 1124–1156, Dec. 2023, doi: https://doi.org/10.1016/j.egyr.2022.11.173. Available: https://www.sciencedirect.com/science/article/pii/S2352484722025628. [Accessed: Mar. 15, 2024]

[6] K. S. Haran et al., "High power density superconducting rotating machines—development status and technology roadmap," *Superconductor Science and Technology*, vol. 30, no. 12, p. 123002, Nov. 2017, doi: https://doi.org/10.1088/1361-6668/aa833e

[7] J. Lin, D. Liu, and Y. Wu, "Concentric-Coil Distributed Winding Design for Large Direct-Drive Fully Superconducting Machines," IEEE Transactions on Applied Superconductivity, vol. 33, no. 5, pp. 1–5, Aug. 2023, doi: https://doi.org/10.1109/tasc.2023.3248536

[8] M. Zhang, F. Eastham, and W. Yuan, "Design and Modeling of 2G HTS Armature Winding for Electric Aircraft Propulsion Applications," IEEE transactions on applied superconductivity, vol. 26, no. 3, pp. 1–5, Apr. 2016, doi: https://doi.org/10.1109/tasc.2016.2539548

[9] S. S. Kalsi, K. A. Hamilton, and R. A. Badcock, "Superconducting rotating machines for aerospace applications," *2018 Joint Propulsion Conference*, Jul. 2018, doi: https://doi.org/10.2514/6.2018-4796

[10] J.-Y. Lee, G.-D. Nam, I.-K. Yu, and M. Park, "Design and Characteristic Analysis of an Axial Flux High-Temperature Superconducting Motor for Aircraft Propulsion," *Materials*, vol. 16, no. 9, pp. 3587–3587, May 2023, doi: https://doi.org/10.3390/ma16093587

[11] D. Lee, T. Balachandran, H.-W. Cho, and K. Haran, "Exploring Fully Superconducting Air-Core Machine Topology for Off-Shore Wind Turbine Applications," *IEEE Transactions on Magnetics*, vol. 55, no. 7, pp. 1–6, Jul. 2019, doi: https://doi.org/10.1109/tmag.2019.2905591

[12] C. D. Manolopoulos et al., "Comparison Between Coreless and Yokeless Stator Designs in Fully-Superconducting Propulsion Motors," *IEEE transactions on applied superconductivity*, vol. 30, no. 6, pp. 1–7, Sep. 2020, doi: https://doi.org/10.1109/tasc.2020.2992588

[13] P. J. Masson and C. A. Luongo, "HTS Machines for Applications in All-Electric Aircraft," *IEEE Power Engineering Society General Meeting*, Jun. 2007, doi: https://doi.org/10.1109/pes.2007.385622W.-K. Chen, *Linear Networks and Systems.* Belmont, CA, USA: Wadsworth, 1993, pp. 123–135.

[14] T. Balachandran, D. Lee, N. Salk, and K. S. Haran, "A fully superconducting air-core machine for aircraft propulsion," *IOP conference series*, vol. 756, no. 1, pp. 012030–012030, Mar. 2020, doi: https://doi.org/10.1088/1757-899x/756/1/012030

[15] S. S. Kalsi, J. G. Storey, J. M. Brooks, G. Lumsden, and R. A. Badcock, "Superconducting Synchronous Motor Development for Airplane Applications - Mechanical and Electrical Design of a Prototype 100 kW Motor," *IEEE Transactions on Applied Superconductivity*, vol. 33, no. 5, pp. 1–6, Aug. 2023, doi: https://doi.org/10.1109/tasc.2023.3242629

[16] S. P. Colyer, P. Arumugam, and J. F. Eastham, "Modular airgap windings for linear permanent magnet machines," *IET Electric Power Applications*, vol. 12, no. 7, pp. 953–961, Jun. 2018, doi: https://doi.org/10.1049/iet-epa.2017.0668

[17] J. F. Eastham, T. Cox, and J. Proverbs, "Application of planar modular windings to linear induction motors by harmonic cancellation," *IET electric power applications*, vol. 4, no. 3, pp. 140–140, Jan. 2010, doi: https://doi.org/10.1049/iet-epa.2009.0086